Real-Time Operational Forecasting on Shipboard of the Iceland–Faeroe Frontal Variability

A. R. Robinson,* H. G. Arango,* A. J. Miller,+
A. Warn-Varnas,#,& P.-M. Poulain,# and W. G. Leslie*

ABSTRACT

Real-time operational shipboard forecasts of Iceland–Faeroe frontal variability were executed for the first time with a primitive equation model. High quality, intensive hydrographic surveys during August 1993 were used for initialization, updating, and validation of the forecasts. Vigorous and rapid synoptic events occurred over several-day timescales including a southeastward reorientation of the Iceland–Faeroe Front and the development of a strong, cold deep-sock meander. A qualitative and quantitative assessment of the skill of these forecasts shows they captured the essential features of both events. The anomaly pattern correlation coefficient and the rms error between forecast and observed fields are particularly impressive (and substantially superior to persistence) for the forecast of the cold meander.

1. Introduction

Oceanic synoptic–mesoscale variability is dynamically analogous to atmospheric synoptic-scale phenomena and represents the internal weather of the sea. Prediction of ocean mesoscale variability is interesting and important for both scientific and application purposes. Although rapid progress is occurring in ocean forecast research, oceanographers are still far behind meteorologists in their numerical weather prediction capabilities. We report here the successful results of real-time shipboard forecasting of vigorous mesoscale meandering and eddying of the frontal system between Iceland and the Faeroe Islands, called the Iceland–Faeroe Front (IFF).

The forecasts were performed onboard ship [the NATO (North Atlantic Treaty Organization) research vessel *Alliance*] and in real time during 15–24 August 1993. A primitive equation numerical model was used and data assimilation was carried out with an optimal interpolation scheme. The forecasts were of 7 days duration and were performed in an operational mode; that is, they were issued according to a regular and preset schedule. Data for model initialization, updating, and verification were gathered by the ship. Auxiliary forecasts were also carried out with a quasi-geostrophic model and a coupled surface boundary layer model driven by atmospheric fluxes. Using the forecasts by the primitive equation model as input, forecasts of time- and range-dependent acoustic propagation were executed with a parabolic equation acoustical model.

Oceanographers commonly refer to the energetic variability, which occurs on spatial scales characterized by the internal Rossby radius of deformation, as mesoscale variability (Robinson 1983), although the scientific analog is to the atmospheric synoptic scale. The internal radius in the ocean ranges from less than 10 km to several tens of kilometers and thus is two orders of magnitude or more smaller than the internal radius in the atmosphere. In the Iceland–Faeroe region the internal radius is only approximately 10 km. The small spatial scale of the variability makes research difficult and the development of forecasting a challenging task. Although realistic global- and ba-

*Division of Applied Sciences, Department of Earth and Planetary Sciences, Harvard University, Cambridge, Massachusetts.
+Scripps Institution of Oceanography, La Jolla, California.
#SACLANT Undersea Research Centre, La Spezia, Italy.
&Naval Research Laboratory, Stennis Space Center, Minnesota.
In final form 5 June 1995.
Corresponding author address: Prof. Allan R. Robinson, Division of Applied Sciences, Pierce Hall, Harvard University, Cambridge, MA 02138.

sin-scale ocean forecasts with mesoscale resolution are not yet feasible, regional forecasts are. Timescales of ocean mesoscale variability range from days to months. Because the variability is episodic and intermittent, an oceanic region is generally characterized by two timescales, one for the evolution and propagation of features and a second shorter one for the occurrence of energetic synoptic dynamical events. Such events—for example, the rapid nonlinear cresting of a meander or the snapping off of a ring eddy from a current—are generally localized and may be referred to in the spatial sense as submesoscale. Two timescales are known to characterize the Iceland–Faeroe frontal region where bursts of baroclinic instability cause rapid evolution (Miller et al. 1995a,b).

From a scientific viewpoint, nowcasting and forecasting oceanic mesoscale variability is important in order to efficiently use research resources in the intermittent ocean. Forecasting knowledge allows for the effective use of resources by "going to the right place at the right time." Nowcasts and forecasts are essential for the rapid assessment of a region for naval operations. Environmental factors associated with the water column, such as thermal gradients, can affect, for example, the distribution of free-floating mines or antisubmarine warfare tactics. Transport and distribution of nutrients and pollutants require forecasting in areas of coastal zone and fisheries management. General management and operational applications are discussed by Durham and Lewis (1992) and Peloquin (1992) in introductions to special issues of the *Marine Technology Society Journal* and *Oceanography,* respectively, which provide good reviews of the field. The real-time shipboard problem is introduced by Robinson (1992). Although mesoscale forecasting research is only about a decade old (Mooers et al. 1986), operational forecasts have been initiated for the Gulf Stream region (Clancy 1992). This is the region where a relatively good quality dataset (Lai et al. 1994) has also been assembled for forecast and simulation validation, and preliminary results are presented by Willems et al. (1994).

In this paper we describe, interpret, and evaluate the real-time primitive equation (PE) forecasts with optimal interpolation (OI) data assimilation made for the Iceland–Faeroe frontal system in August 1993. To our knowledge, it is the first time such forecasts have been made onboard ship and in an operational mode. Moreover, the forecast experiment was designed to acquire adequate data for PE model assimilation and verification. Unusually good weather allowed the ship to acquire the complete, accurate high-resolution dataset for these purposes. Several-day forecasts validate successfully both qualitatively and quantitatively, with the occurrence of two vigorous synoptical–dynamical events that were not present in initialization data. A rapid straightening and shifting of the frontal current was followed by the development of an intense deep-sock meander. The term "sock" describes the meander's general shape and has been in use since the early 1960s (Fuglister 1963).

In the following, we review the phenomenology of the IFF system, present the data and describe the synoptic variability observed, discuss forecast methodology, present and evaluate the forecasts, and discuss conclusions.

2. The Iceland–Faeroe frontal system

The IFF is located between Iceland and the Faeroe Islands in a region where the ocean bottom rises to within 400 m of the surface. The front forms the intersection of the warm saline North Atlantic water mass and the cold low-salinity Arctic water mass. Strong currents and sharp temperature gradients are found in this area. The classic picture of the temperature front in summer is shown in Fig. 1, from the 1958 International Geophysical Year surveys (Dietrich 1969).

From various studies, a composite picture of the current structures has emerged that shows a flow along the frontal area with inflow from the North Atlantic along the southeastern Icelandic shelf. Some inflow of Arctic-type water occurs along the northeastern Icelandic shelf and merges with the North Atlantic water inflow at the frontal location off Iceland (Peggion 1991). In the frontal region, a high degree of mesoscale dynamical activity exists. Frontal meanders and cold and warm eddies are present. Atmospheric cooling, mixing of the upper ocean, internal tides, and waves occur.

In the last few decades, a multitude of efforts for describing the thermal and current structures in the IFF have been conducted. These efforts began with the interpretations of the 1960 Overflow Expedition data by Hansen and Meincke (1979), who showed the existence of cold anomalies south of the IFF and warm ones just north of it. Hansen and Meincke proposed that the anomalies were caused by rapidly changing mesoscale eddies. This conjecture remained to be verified, as the 1960 Overflow Expedition surveys did not map the mesoscale field with sufficient resolution.

Studies of current meter data from the Monitoring the Overflow in the North Atlantic (MONA) project reveal that the timescale of subtidal fluctuations is on the order of a few days (Willebrand and Meincke 1980). The correlations between the velocity and temperature time series imply that there is conversion from mean potential energy to eddy kinetic, an expression of the baroclinic instability process.

Subsequent surveys and studies increased the documentation of the complicated eddy and frontal structures in the IFF (Smart 1984; Gould et al. 1987; Scott and McDowall 1990; Hopkins 1991; Niiler et al. 1992; Read and Pollard 1992; Perkins 1992; Allen et al. 1994; Miller et al. 1995a,b). The fine-resolution sections of these experiments were in the range of 4–7 km along tracks and 16–24 km between them. This enabled the quantification of the size and strength of the mesoscale and studies of the IFF dynamics. Denbo and Robinson (1988a,b) obtained a coarse mesoscale resolution time series of synoptic realizations of the IFF and initiated quasigeostrophic forecast experiments.

From the data, a picture of the eddy population in the IFF region is starting to emerge. Interpretation of the survey conducted by Gould et al. (1987) shows 7 cold eddies south of the IFF; Niiler et al. (1992) and Scott and Lane (1990) located 10 cold eddies of 30–50-km size and only 1 warm eddy north of the IFF. Allen et al. (1994) found a number of cold-core cyclonic eddies of 15–30 km and a few warm anticyclonic features. For the interpretation of the statistics of the data, Niiler et al. (1992) suggest that the dynamical situation for cold eddy formation is analogous to that of the Gulf Stream.

Recently, Miller et al. (1995a) have extended the synoptic description of the IFF evolution further by a direct model simulation of an observed instability. A typical rapid growth cold-tongue intrusion observed along the IFF, during a cruise in the fall of 1992, was diagnosed to be due to a baroclinic instability mechanism. It was shown that energy is drawn from the mean vertical shear at middepth and transferred to the mid- and upper-level kinetic energy. The effects of topography are minimized because the burst instability mechanism appeared to be surface intensified and occurred very rapidly in a submesoscale region.

3. Data and objective analysis maps

In August 1993, the Supreme Allied Commander, Atlantic (SACLANT) Undersea Research Center (SACLANTCEN) and Harvard University performed a joint hydrographic survey of the IFF for the purposes of real-time nowcasting and forecasting of IFF variabilities and studies of physical processes within the region (Poulain 1993; Robinson et al. 1994).

The general location of the experiment is shown in Fig. 2a, in which is outlined the observational and modeling domain, centered at 64.25°N, 10.75°W and 140 km in longitudinal extent and 190 km in latitudinal extent. This domain is enlarged in Fig. 2b, which shows the detailed underlying bottom topography that is input to the model. The experimental domain is essentially located on the top of the Iceland–Faeroe Ridge that descends into the Greenland–Iceland–Norway (GIN) Sea to the north and the North Atlantic to the south. Except for the northeast corner, the forecast domain is fairly flat in the south (about a 500-m depth) and uniformly sloped up to the west in the north. The model topography has been smoothed and conditioned (Lozano et al. 1994), which can limit a model's ability to capture certain small-scale dynam-

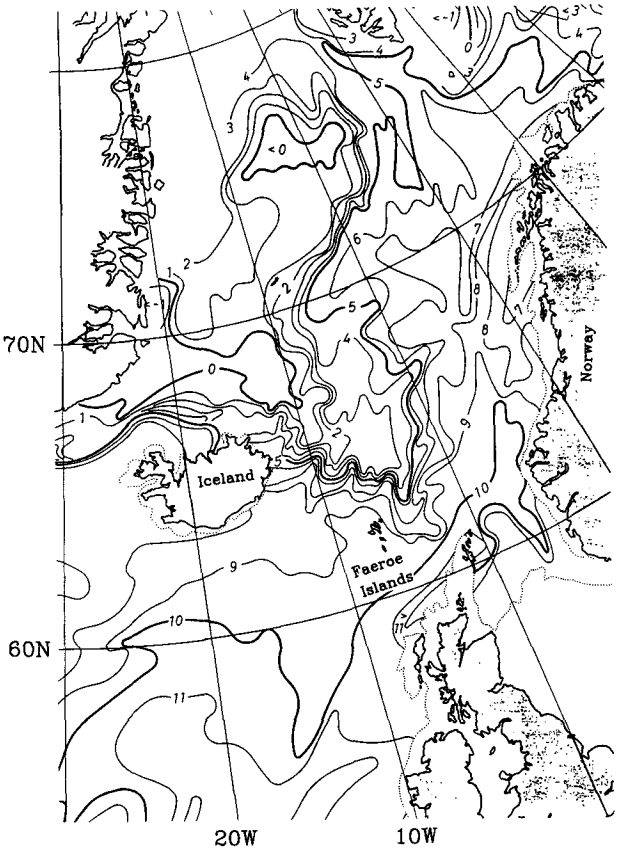

FIG. 1. Temperature at 100 m during the summer in the region of the Greenland–Iceland–Norway Sea. Contour interval is 1°C (from Dietrich 1969).

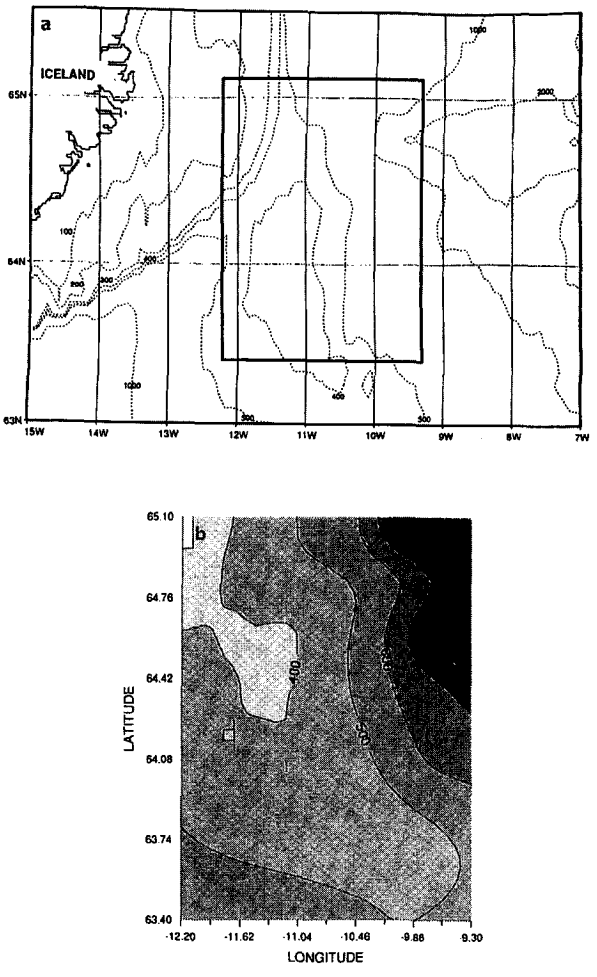

FIG. 2. (a) Map of the topography southeast of Iceland, showing the model domain (inner box). (b) Smoothed and conditioned topography used in the domain of the primitive equation model (Contour interval is 100 m).

ical events, such as density-driven overflows through narrow topographic gaps. Our model, on the other hand, feels the larger-scale dynamical effect of this topography as it affects the barotropic and baroclinic evolution of the unstable IFF current. Since the IFF current and its associated eddy field tends to be surface intensified, our smoothed rendition of the true topography will have a satisfactory dynamical effect on the anticipated mid- to upper water column burst instability events that are known to occur in this region and that result in the ambient eddy field. Furthermore, although our hydrographic sampling grid was not designed to properly resolve possible deep overflow events through narrow gaps, those thermohaline events are rare and are probably not directly coupled to the larger-scale IFF current variations that the model is fully capable of simulating.

The expendable bathythermograph (XBT), conductivity–temperature–depth (CTD), and expendable CTD (XCTD) data were grouped into three separate surveys (Figs. 3a–c), hereinafter referred to as the initialization, zigzag, and validation surveys. The subdomains on Figs. 3b,c are forecast evaluation domains to be described in section 6. Besides the hydrocasts, we deployed two sets of surface drifters (Poulain 1993) in the axis (18–19 August) of the IFF. One clear satellite image of SST in the survey area was also available for 22 August (Fig. 5).

To optimize the potential for quantitative forecast verification, the sampling locations and ship tracks of the initialization and validation surveys were identical. Since the ship entered the experimental domain from the east, the patterns were occupied from east to west. The zigzag survey was designed in real time to pinpoint forecast positions of the IFF during nighttime operations, while current meter moorings were being recovered during daylight. As the mooring data were not telemetered, it was not possible to use the data during the real-time forecasting. An analysis of the mooring data has been performed by Miller et al. (1995c).

The initialization survey spanned 14–16 August and included XBTs, XCTDs, and CTD data (Fig. 3a), sampled at a 24-km resolution in the east–

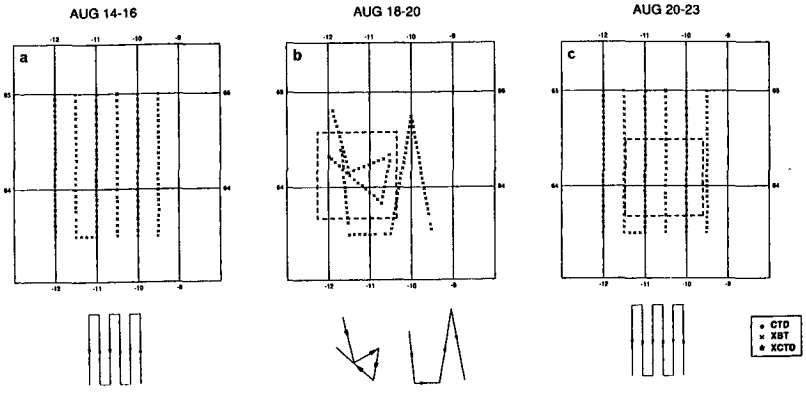

FIG. 3. Maps of the locations of the hydrographic surveys during the August 1993 cruise for (a) initialization survey, (b) zigzag survey, and (c) validation survey. The type of data acquired (XBT, CTD, XCTD) is indicated by a symbol. The path followed during the survey is sketched in the diagram beneath each figure. The subdomains in (b) and (c) are used for validation.

west direction and approximately a 7-km resolution in the north–south direction along track. The zigzag survey, from 18 to 19 August, consisted solely of XBTs in and around the western central part of the IFF (Fig. 3b). The validation survey, during 20–23 August, charted the same track as the initialization survey, albeit at a slower pace, because it included more CTDs among the hydrocasts (Fig. 3c). Once the data were collected and visually preprocessed (for obvious errors), the XBT data were supplemented with salinity data that were derived from a temperature–salinity (T–S) water mass model (Robinson et al. 1994). This water mass model was constructed during the cruise and used the CTD and XCTD salinities gathered in real time. As the water mass composition of each XBT was identified, salinity appropriate to that water mass, as measured on the cruise, was added to the XBT temperature information (with appropriate density constraints).

The synoptic observations for the three surveys are summarized in Fig. 4 in terms of temperature maps near the surface (25 m), upper water column (125 m), and deeper water column (level 4). The deeper map was prepared for assimilation in, and evaluation of, the dynamical model that uses a terrain-following ("sigma") coordinate system, which is explained in the next section. Sigma levels are not horizontal. The deeper water temperature map is predominantly located between 200 and 300 m (~220 m, but not exactly), but with a slope downward to the northeast.

The time-dependent objective analyses used an isotropic autocorrelation function of the form

$$C(r,\delta t)=\left[1+\left(\frac{r}{a}\right)^2\right]e^{-\frac{1}{2}\left(\frac{r}{b}\right)^2}e^{-\frac{1}{2}\left(\frac{\delta t}{c}\right)^2}+\sigma^2\delta_{ij}. \qquad (1)$$

Here r is a spatial lag vector having a magnitude of

$$r=\left[\left(x_i-x_j\right)^2+\left(y_i-y_j\right)^2\right]^{\frac{1}{2}},$$

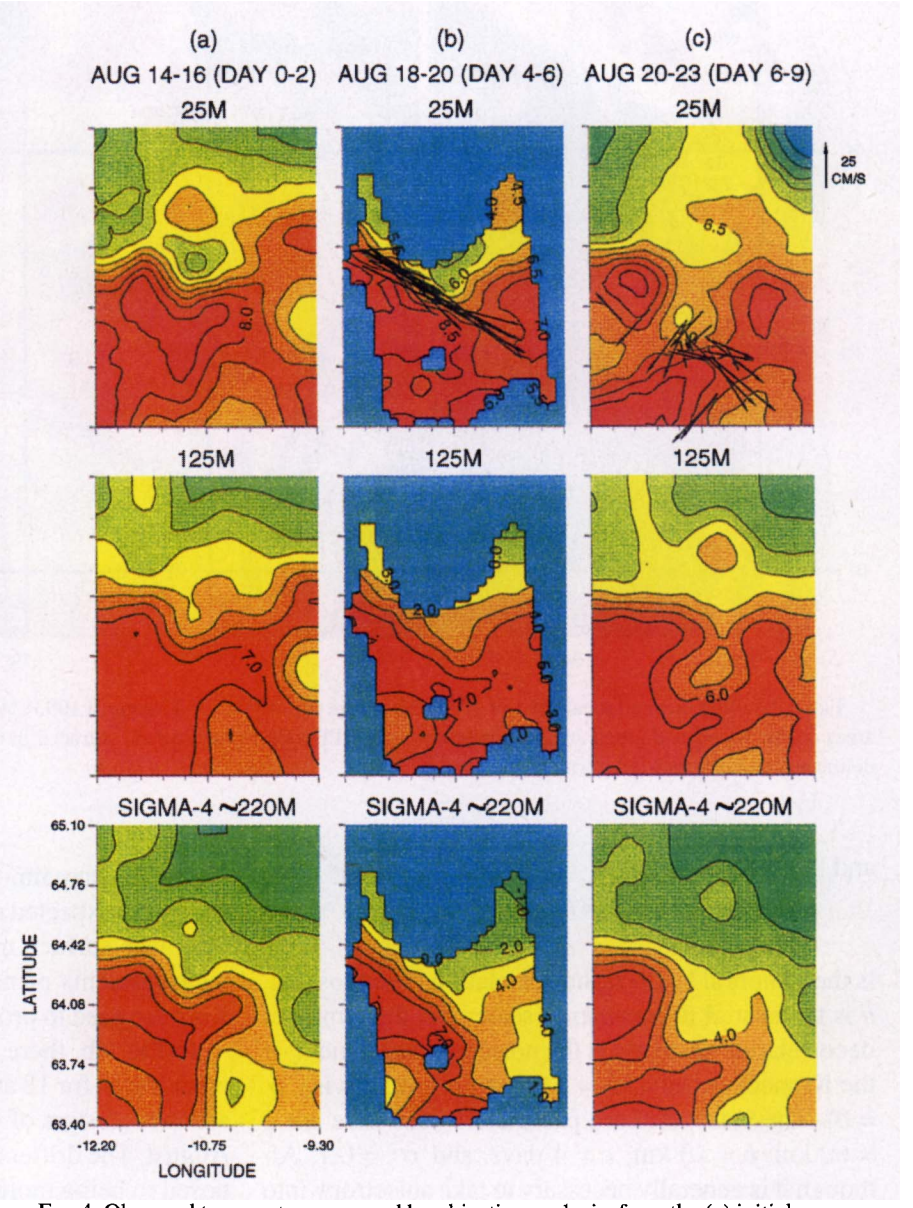

FIG. 4. Observed temperature, mapped by objective analysis, from the (a) initial survey, (b) assimilating zigzag survey, and (c) validating survey at (top) 25 m, (middle) 125 m, and (bottom) the sigma-coordinate level that varies from a 180- to a 300-m depth. At 25 m, the contour interval is 0.5°C. At 125 m and at sigma 4 (~220 m), the contour interval is 1°C. Surface drifter velocity observations (inferred from 12-h displacements, drogued to a 15-m depth) are shown for 18 and 19 August on the zigzag survey and for 21 and 22 August on the validation survey.

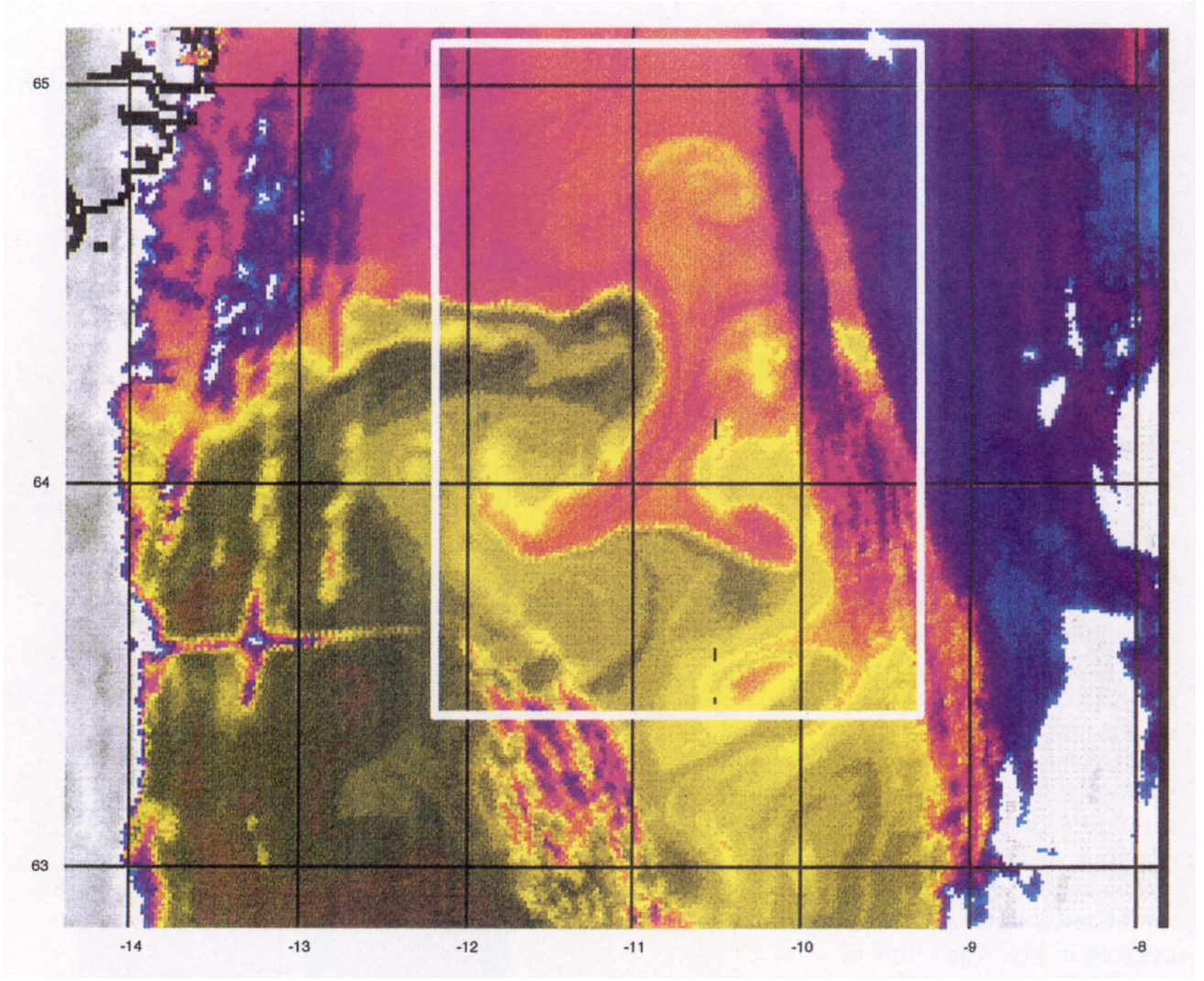

FIG. 5. Satellite infrared (channel 4 of AVHRR) image for 1431 UTC 22 August 1993 . White and blue areas indicate clouds, pink areas cooler water, and green areas warmer water. The PE forecasting domain is traced in the image. Part of the coast of Iceland is delineated in the upper-left corner.

and

$$\delta t = t_i - t_j$$

is the temporal lag, a is the correlation zero crossing, b is the spatial decorrelation scale, c is the temporal decorrelation scale, σ^2 is the noise variance, and δ_{ij} is the Kronecker Delta ($\delta_{ij} = 1$ when $i = j$; otherwise, $\delta_{ij} = 0$). The value of these parameters used here are $a = 60$ km, $b = 40$ km, $c = 4$ days, and $\sigma^2 = 0.1$. Although it is generally necessary to take anisotropy into account in the vicinity of a jet, the dense data coverage allowed the use of an isotropic correlation function. In cases with dense sampling, the objective analysis scheme acts as a simple interpolator. The maps are for the central day of each survey, that is, 15, 19, and 22 August. Since the zigzag survey did not cover the entire domain, the maps of Fig. 4b are masked where the expected error of the analysis exceeds 25%. The near-surface maps also present surface drifter measurements of near-surface velocity; the drifters were drogued to provide the velocity at a 15-m depth.

In Fig. 4b, there are two clusters of 6-h displacement tracks for 18 and 19 August, and in Fig. 4c there are two clusters of 6-h displacements for 21 and 22 August. The drifters were launched as clusters, as opposed to being more widely dispersed, in order to investigate the dispersion about a center of mass and to provide information regarding divergence, convergence, vorticity, etc. By preceding the launch of the drifters with the first hydrographic survey, the drifters were able to be located close to the frontal axis in the most interesting location.

Near the surface and in the upper water column, the frontal and eddy fields are quite similar. However, there are distinct differences at depth in the central and eastern regions of the domain. Note that the inlet position of the front on the western boundary is nearly stationary throughout the experiment. On 15 August (Fig. 4a), the IFF was oriented eastward in a distinct meander pattern with a crest at about 11.5°W longitude and a trough at about 11°W. In the east, in the upper ocean (Fig. 4a; 25, 125 m), the flow broadens and bifurcates around a pair of eddies only partially contained within the domain. In the deep ocean, the front flows to the south, where it exits the domain. The general orientation and location of the deep front remained constant throughout the experiment but was accompanied by vigorous meandering (Figs. 4a,c at ~220 m). The upper frontal system evolved rapidly and changed qualitatively between each survey. By 19 August (Fig. 4b; 25, 125 m), the meander had disappeared, and the straightened frontal stream had shifted to a southeastward orientation in the western domain and a northeastward orientation in the eastern domain. However, only 3 days later, on 22 August (Fig. 4c; 25, 125 m), the dominant synoptic feature was a large cold intrusion or deep-sock meander, which had developed in the center of the domain. The center of the intrusion is shifted about 0.5° of longitude westward at 25 m relative to 125 m, and the near-surface meander is surrounded by a pair of strong, warm eddies. The drifter observations generally affirm the structure of the feature, flowing southwestward along the western border on 21 August followed by an eastward flow along the base on 22 August with a subsequent entrainment in the southward branch of the bifurcating flow. The satellite-observed sea surface temperature (Fig. 5) confirms unambiguously the existence of the deep-sock, or hammerhead, nonlinear meander.

4. Forecast methodology

The Harvard Ocean Prediction System (HOPS) is an integrated system of software developed in general for producing interdisciplinary oceanic field estimates, including nowcasts, forecasts, and data-driven simulations from a variety of data types and databases (Harvard Group 1994; Robinson 1993; Robinson et al. 1994). The general configuration is shown schematically in Fig. 6. It is a flexible, portable system whose modularity facilitates efficient configuration for specific applications. For the real-time operational forecasts aboard the R/V *Alliance* in August 1993 the configuration included modules for hydrographic data analysis; Lagrangian drifter analysis; objective analysis; optimal interpolation; climatology, correlation statistics, and a feature model for the IFF frontal current; primitive equation dynamics; and visualization. The Geophysical Fluid Dynamics Laboratory primitive equation model (Bryan and Cox 1967; Semtner 1974) provides the basic integration algorithm for the open boundary PE model used for HOPS. The PE open boundary conditions, subgrid-scale physics, and

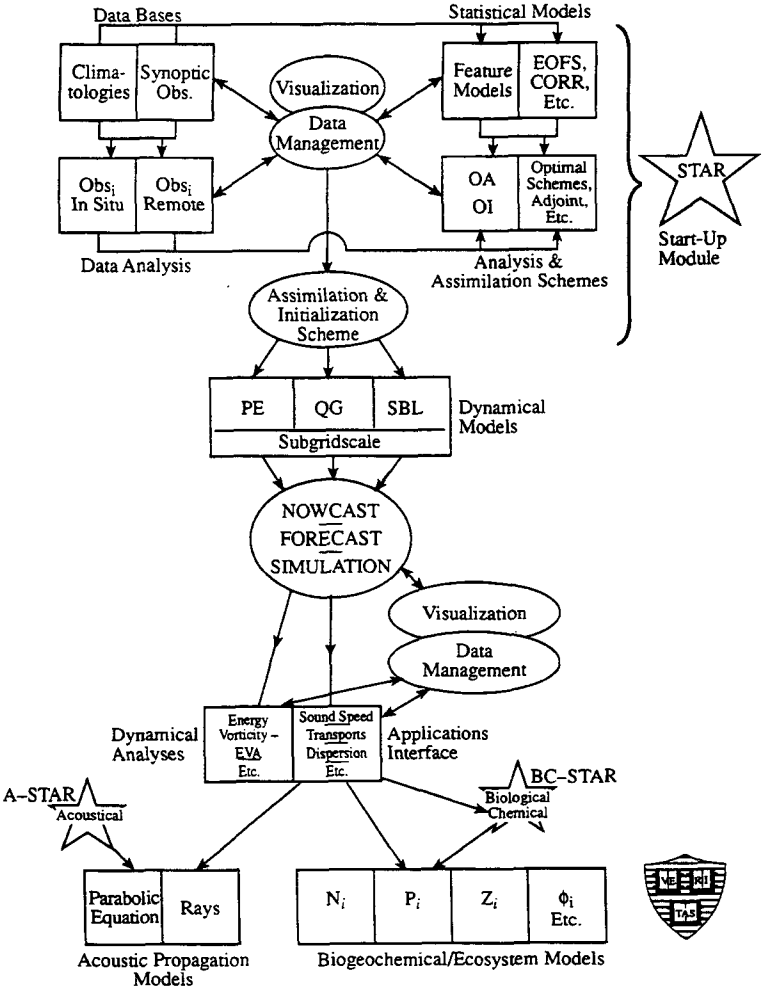

FIG. 6. Schematic of HOPS, the Harvard Ocean Prediction System.

bottom topographic treatment via hybrid coordinates were developed at Harvard; Spall and Robinson (1989) present the documentation and calibration. The PE integration algorithm has been modularized, and the pressure gradient algorithm replaced by one that maintains accuracy and efficiency in the presence of very steep and tall topography (Lozano et al. 1994).

The hybrid coordinate system consists of level surfaces in the upper ocean down to a prescribed depth below which a terrain-following sigma coordinate system is used. Sigma coordinates are gradually influenced by the shape of the bottom and a level sigma surface coincides with the bottom at the bottom. The PE model was set up with five "levels" in the vertical, horizontal surfaces at 25, 75, and 125 m and sigma surfaces located predominantly at ~220 and ~350 m, but with a pronounced downward slope localized in the northeast corner and a slight slope downward in the southeast corner. The horizontal resolution was 5 km, and the time step was 30 min. The subgrid-scale dissipation was accomplished by a Shapiro filter of order 4 applied five times each time step to the momentum and temperature equations. This is a weak filter, and for short forecasts there is little sensitivity to a reasonable range of filter parameters.

The PE model forecasts were driven by initial conditions, boundary conditions, and updating. The regional fields, as part of a larger-scale circulation system, evolved via internal dynamical processes. Local direct atmospheric forcing was neglected in the PE forecasts, which is an approximation that was consistent with the light and nearly constant winds experienced. Hydrographic data provide temperature and salinity directly for assimilation, and geostrophic computations provide the zero-depth-average internal velocity mode. The depth-averaged velocity, the barotropic or external mode, was inferred from geostrophy plus surface drifter information, which became available first on 18 August. The measured barotropic mode implied a surface geostrophic velocity that was 1.25 times the value of the surface value calculated relative to the bottom, which had been used prior to the availability of float data.

We term our general shipboard methodology to build and maintain a synoptic description of an oceanic region, primarily using in situ data obtained by the ship itself as it moves around the forecast region, as "sequential updating." A subdomain of the entire region is first analyzed when sufficient data have been obtained to make a reasonable nowcast. With a dedicated research vessel taking hydrographic observations with a mix of CTDs and expendable probes, this is typically 1 day's (24 h) worth of data. Given the differences between oceanographic and atmospheric event scales, 1 day for the ocean is comparable to 6 h for the atmosphere. When the first subdomain data are available, the entire domain is initialized, using in the data-empty region elements from the regional historical synoptical database, for example, a gridded climatology and/or feature models representing typical synoptic coherent structures. On successive days, as new subdomain datasets become available, they are assimilated via optimal interpolation into nowcasts. In this way, the entire domain is built up, with data being assimilated and evolving as synoptically as possible. When data have been collected over the entire domain, meaningful forecasting can begin. As the ship continues to operate in the region, the sequential assimilation procedure is continued whenever sufficient data are obtained over a subdomain to make updating meaningful. This methodology allows for initial analysis and nowcasting as soon as is possible.

The specific initialization and assimilation strategy for this experiment was as follows. We designate 14 August as day 0. The initialization survey took 3 days to accomplish (day 0, 1, 2) as the ship moved from east to west. The model was first initialized on day 0, with the strip (or slab) of data available in the eastern third of the domain. In the central and western areas of the domain, initialization consisted of a feature model representation of the frontal fields along the mean east–west axis of the stream, with estimated mean stratification to the north and south. The feature model is explained in the next section. When the central strip of data became available for day 1, it was assimilated via optimal interpolation, as was the day 2 data. Thus, the forecast domain was built up by a process of initialization on day 0, followed by two cycles of intermittent optimal interpolation on days 1 and 2. The field estimates from melded data and dynamics on days 0, 1, 2 we designate as nowcasts. The forecast carried out from this buildup process is designated as F2 (the last day of data assimilation). Zigzag survey data became available on day 5. The forecast carried out with the assimilation of this data is designated as F5. The OI assimilation weights were based primarily on the three-dimensional expected error distribution of the objectively analyzed (OA) maps of the data. The minimum observational error was 0.1, which was taken to correspond to an observational weight of 0.9. The OA

maps then produced the data weights to estimate the field $F_{est} = W_o F_{obs} + W_f F_{forecast}$, and the forecast weight was simply $W_f = 1 - W_o$. For F5, the zigzag data were treated as a damped assimilation and ramped up and down in time with maximum weights of 0.4 on day 4, 0.8 on day 5, and 0.4 on day 6. The open boundary conditions were, as usual, specified as inflow and outflow, with temperature, salinity, and tangential velocity specified on the inflow (Spall and Robinson 1989). During the nowcasts and forecasts, all boundary conditions were persisted except during an assimilation cycle. Although the zigzag survey maps (Fig. 4b) are masked at 25% error, the assimilation of the survey was carried out over the entire domain, including boundary updating. Development of the technical details for a successful methodology of east–west domain buildup with OI data assimilation was carried out via an Observation System Simulation Experiment (OSSE) reported by Robinson et al. (1994) based on data from a 1992 cruise to the IFF (Poulain 1992; Miller et al. 1995a).

Real-time operational nowcasts and forecasts of 7-day duration were issued on 16, 17, 19, 20, 21, and 23 August and delivered to the scientist-in-charge of the R/V *Alliance*. Those at-sea nowcasts and forecasts were used to determine existing conditions and evaluate positioning for upcoming work. Though not presented here, the forecasts are all similar to either F2 or F5 described above and discussed in the next section except for the final forecast that assimilated some validation survey data. The forecasts were carried out on two SUN SPARC-10 workstations brought aboard the R/V *Alliance* from Harvard University. The hydrographic data were collected, calibrated, and quality controlled by the SACLANTCEN scientific and technical group and then transferred to the Harvard modeling group. Drifter locations were obtained daily from Argos. The data were available from the SACLANTCEN group within 8 h of being collected, and subsequent processing for modeling work was completed within the next 3–12 h. The processing could be a lengthy procedure due to the quantity of data and the complexity of dynamical features contained therein. The average forecast took from 20–40 min on the SPARC stations for forecasts of 1–2 weeks duration.

5. Forecasts

Results for the nowcasts of days 0 and 2, F2 forecasts for days 5 and 8, and the F5 nowcast for day 5 and forecast for day 8 are presented in Figs. 7, 8, and 9, respectively. In each case, the temperature nowcasts and forecasts are shown for the near-surface and upper-ocean horizontal levels (25 m, 125 m) and the deeper sigma model level 4, predominantly located at 200–300 m, to facilitate comparison with the observations presented in Fig. 4. The predicted surface velocity vectors are overlaid on the near-surface temperatures.

a. Nowcasts for 14 and 16 August (days 0, 2)

Looking first at the nowcasts, day 0 (Fig. 7a) depicts the dynamically adjusted feature model initialization in the western and central domains, melded with the initialization via observations in the eastern domain. In this case, the feature model was constructed from a set of pseudo-observations. From the true observations in the eastern domain, a typical Atlantic water CTD cast and a typical Arctic water CTD cast were constructed, which were then used to construct a "pseudodataset" for central and western regions that had not yet been sampled. The axis of the front was located in a climatological mean position and a typical synoptic frontal width specified by including an appropriate distribution of pseudodata, which were then objectively analyzed over the entire domain for the day 0 nowcast initialization. A similar procedure was used for the day 1 nowcast.

Our use of feature models, in this region, for the representation of synoptic structures from sparse data, dates back to 1988 (Denbo and Robinson 1988b). While the chosen feature models for this work are semianalytical, digital feature models for the regional structures (Bennett et al. 1992) also exist. By combining the real-time observations with analytical models, an accurate picture of synoptic conditions can be generated.

The day 2 nowcast (Fig. 7b) has assimilated, via intermittent optimal interpolation in three daily cycles, the entire initialization survey dataset. It represents a field estimate in which synoptic data have been assimilated synoptically, dynamically adjusted, dynamically interpolated, and dynamically extrapolated. It should be compared with the objective analysis for the central day of the survey (Fig. 4a). Although a time-dependent OA was used, since every region of the domain was sampled only once, the full domain maps for day 0, 1 (not shown) are essentially identical to the day 2 map (Fig. 4a). What differs from day to day are the maps of expected error of the analyses. The OA and nowcast estimates of Figs. 4a and 7b are similar, but there are significant differences. In the nowcast, at 25 m, the meander in the west has already partially

collapsed, and at 125 m the meander crest has smoothed, and the trough has weakened and propagated westward. The deeper-level estimates at ~220 m do not noticeably differ. We believe that these dynamical adjustments are real and that the nowcast estimate based on synoptically assimilated data melded with dynamics provides the most realistic picture of the frontal system.

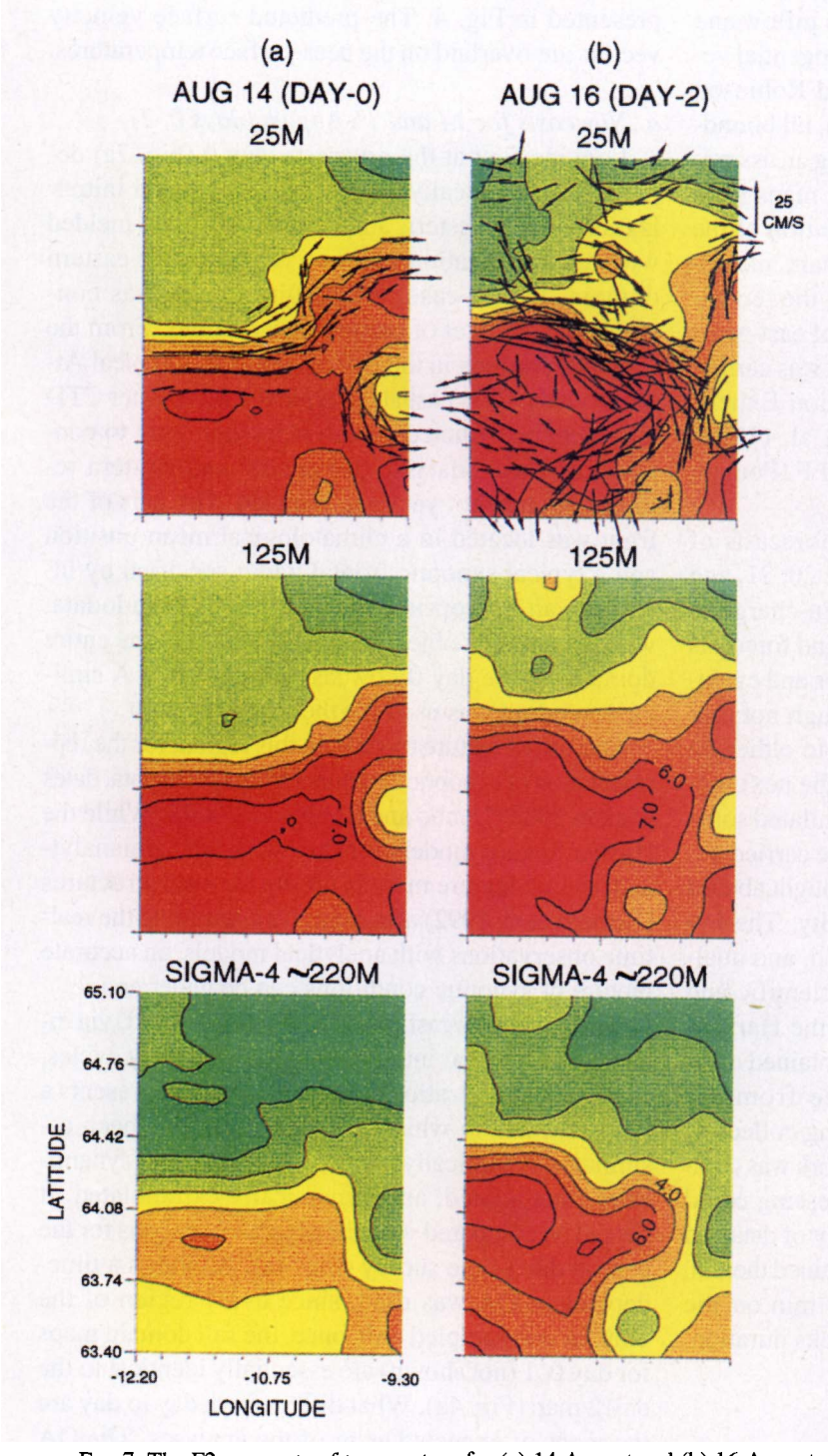

FIG. 7. The F2 nowcasts of temperature for (a) 14 August and (b) 16 August from the PE model, which assimilated data through 16 August, together with a feature model of the IFF. The velocity field for the top layer is also shown, otherwise plotted as in Fig. 4.

b. F2 forecasts and F5 nowcast for 19 August (day 5)

The F2 forecasts shown in Fig. 8 are regarded as initialized by the day 2 nowcast, and thus, the day 5 forecast of Fig. 8a is referred to as a 3-day forecast, and the day 8 forecast of Fig. 8b as a 6-day forecast. Evaluation of the 3-day forecast is possible within the masked region of Fig. 4b. The dynamics have successfully predicted the straightening and southward reorientation of the front in the western domain at all levels. The general northeastward orientation in the eastern domain at 25 and 125 m is also indicated in the forecast field, but at 25 m the prediction includes an unobserved meander pattern, which may well be due to the persistence of the day 2 boundary conditions on the eastern boundary. In the deeper ~220-m level, the persisted southern boundary condition is apparently causing local distortions and features. It is interesting to compare the F2, day 5 forecast (Fig. 8a) with the F5, day 5 estimate (Fig. 9a). Since the F5, day 5 estimate (Fig. 9a) has assimilated the zigzag survey with strong weights within the unmasked region of Fig. 8b, the Fig. 9a maps cannot, of course, be compared to the Fig. 8b maps. It is, however, interesting to note the difference in eastern and southern boundary regions of Figs. 8a and 9a that occurs from boundary updating under the influence of the zigzag data.

c. F2 and F5 forecasts of 22 August (day 8)

The 6-day F2 forecast and the 3-day F5 forecast for 22 August are shown in Figs. 8b and 9b, respectively. In both cases, the dynamics have developed an intense cold intrusion as observed in the validation survey (Fig. 4c). In both forecasts, the southward penetration of the intrusion agrees with observations, but the center is located a little eastward of

the observations, especially F2. Both are colder than observed, and F2 is oriented southeastward of the observations, while F5 has a small eastward protrusion not in the data. The agreement of both forecasts at 125 m is remarkably good. The location of the feature in F5 is excellent, and the only noticeable difference from observations is a nonlinear distortion on the western flank of the meander. The F2 feature is slightly too cold and displaced eastward of the data. The agreement between the F2 and F5 forecasts and the deeper data is also very good. The main difference is the meander amplitude, which is largest in the data (Fig. 4c, ~220 m), less in F5 (Fig. 9b, ~220 m), and weakest in F2 (Fig. 8b, ~220 m), which also has a contaminated southern boundary condition. Qualitatively, the dynamical prediction of this rapid and energetic event is very successful. Next we attempt to quantify the evaluation.

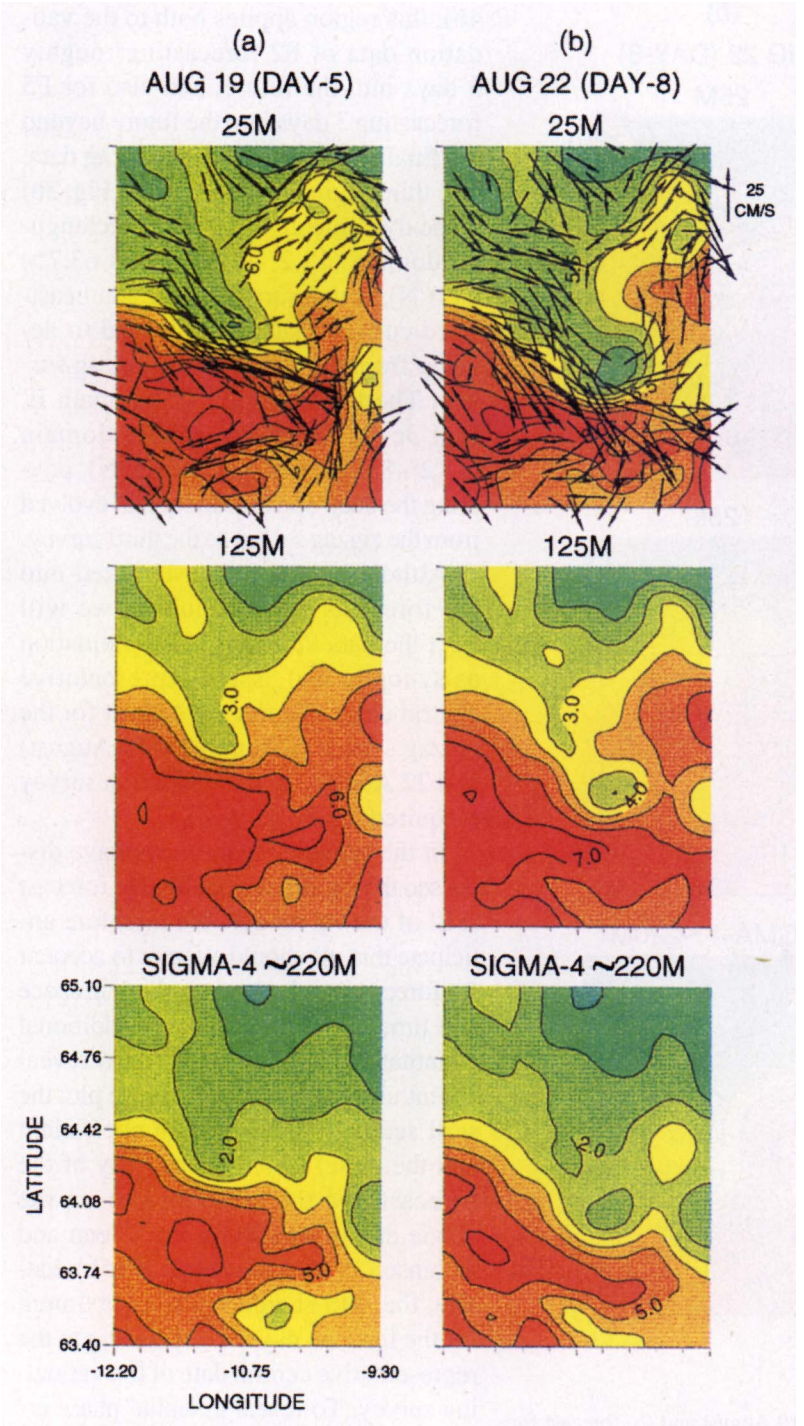

FIG. 8. The F2 forecasts of temperature for (a) 19 August and (b) 22 August for the PE model. Otherwise, as in Fig. 7.

6. Quantitative evaluation

Quantitative demonstrations of ocean mesoscale forecast skill are rare (e.g., see the special issue of *Oceanography* 1992, edited by R. A. Peloquin), and our results in this section are novel. Lynch (1995) provides an overview of the problem from a coastal ocean viewpoint. The sparseness of oceanic data, compared to atmospheric data, makes the verification problem generally very different. Often the lack of sufficient data requires one to devise clever measures of useful skill, such as mean frontal axis position error (Willems et al. 1994) or eddy-spawning event statistics (Robinson et al. 1989). Because we have such unprecedentedly complete initialization and validation information, we adopt the standard statistical validation measures, anomaly correlation coefficient and root-mean-square error (rmse),

$$\mathrm{ACC} = \frac{\langle T_p' T_p' \rangle}{\left(\langle T_p' \rangle \langle T_o' \rangle \right)^{1/2}}, \qquad (2)$$

and

$$\mathrm{rmse} \equiv \left\langle \left(T_p - T_o \right)^2 \right\rangle^{1/2}, \qquad (3)$$

where T_p' is the predicted temperature (with spatial mean removed), T_o' is the ob-

served temperature (with spatial mean removed), and the angle brackets denote averaging over a specified horizontal area. Note that T_p will apply either to the dynamical prediction or to the prediction of persistence of the initial state (i.e., last day of assimilation) against which all measures of quantitative skill will be referenced.

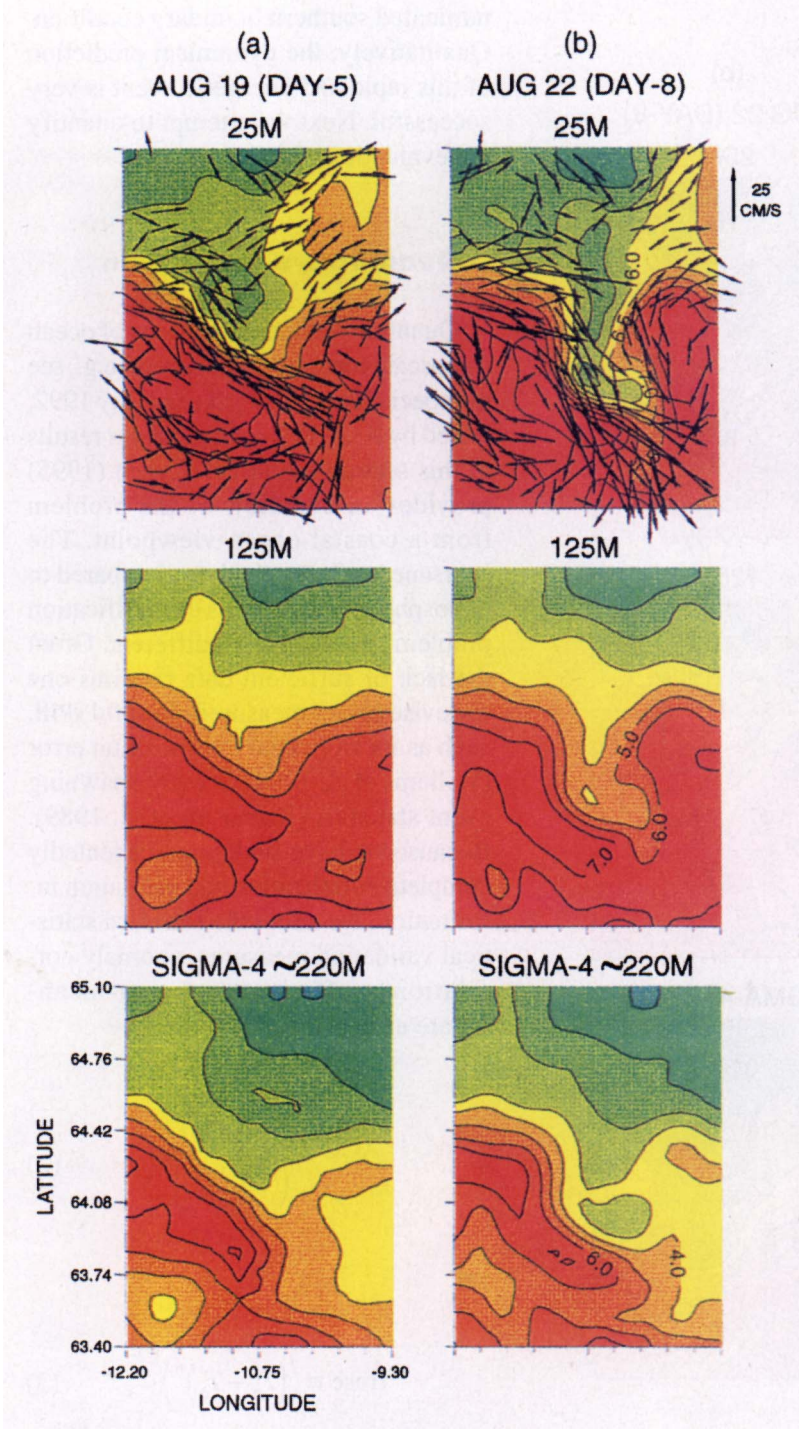

FIG. 9. The F5 (a) nowcast of temperature for 19 August and (b) forecast for 22 August for the PE model, which assimilate all data through 19 August, otherwise as in Fig. 8.

The data coverage, combined with our understanding of what events transpired during the three surveys, causes us to specify four distinct regions in which we can assess the quantitative skill. The first region is the entire model–observation domain (Fig. 2), which applies for F2 forecasting 7 days into the future. The second region is the zigzag area defined by the objective analysis error field (Fig. 4b); this region applies both to the validation data of F2 forecasting roughly 3 days into the future, and also for F5 forecasting 3 days into the future beyond the final assimilation of the zigzag data. The third region (subdomain A, Fig. 3b) is the dynamically interesting rectangular domain (12.2°–10.3°W and 63.7°–64.6°N), which surrounds the southeastward current that was observed to develop from the initial to the zigzag survey. The fourth region (subdomain B, Fig. 3c) is an 85-km-square domain (11.2°–8.3°W and 63.7°–64.5°N), covering the deep-sock meander that evolved from the zigzag survey to the third survey.

Although data was assimilated into the forecasts when acquired, we will treat the data that is used for validation as synoptic and assign representative central dates, namely 19 August for the zigzag survey (acquired 18–19 August) and 22 August for the validation survey (acquired 20–23 August).

In the previous section, we have discussed the significant qualitative forecast skill of the PE model. We therefore anticipate that we should attempt to account for forecasting phase errors, both in space and time, in order to uncover additional quantitative skill information. To reveal potential phase errors in time, we plot the skill scores (for correlation coefficient and the rmse) between each day of the forecast and the observations on the single day of validation (cf. Glenn and Robinson 1995; Miller et al. 1995b). Ideally, the skill should reach a maximum for the forecast day corresponding to the representative central date of the validating survey. To reveal potential phase errors in space, we shift the model prediction (translate the model grid) in both hori-

zontal directions and locate the maximum skill scores. These views of the relation between forecast and observations allow us to identify potential inadequacies in the time evolution of model dynamics, in the sense that, for example, a day $(N+2)$ forecast might be a superior predictor of day (N) observations, indicating that the model eddy features mature too slowly in time or that the fields develop, for example, too far downstream but with accurate spatial fidelity. The treatment of the spatial phase error is fairly crude, as it does not take into account possible pattern rotation, strain, or dilation.

As implied above, the three surveys provide two possibilities for F2 verification and one for F5. We now discuss these in turn.

a. F2 14–16 August assimilation/18–19 August verification

Table 1 shows the difference between the forecast skill and skill of persistence. A positive ACC difference (or a negative rmse change) indicates higher skill for the forecast. Due to the existence of the front, correlations remain high even for persistence forecasts (e.g., typical values of the ACC exceed 0.6 for either model forecasts or persistence of day 0). It should be noted that even a slight improvement in ACC for a forecast can explain a fair percentage of additional pattern variance of the field. For example, if a forecast field has ACC = 0.85, representing an increase of 0.10 over a persistence forecast ACC = 0.75, 16% additional variance of the pattern of the field has been predicted, which is useful. Root-mean-square error, which gives a direct measure of the amplitude discrepancies between forecast and observed, is shown in the tables as a normalized quantity (although it is plotted in subsequent figures in dimensional units).

The most important feature seen in the 18–19 August zigzag survey is the reorientation of the IFF current to a southeastward direction. Table 1 shows that, relative to persistence of the synoptic fields for 14–16 August, the F2 forecast correlates better than the persistence forecast at the top level (25 m) when verifying in the zigzag area. The remaining skill scores in the other levels are inferior to persistence. If we redirect our attention to the region surrounding the southeastward IFF current (subdomain A), we find (Table 1) that the F2 forecast correlates better than persistence at levels 1, 3, and 4. Level 4 also exhibits a reduced rmse relative to persistence. We did not attempt to account for phase errors in space for this case, since it was evident that the southeastward current developed at the correct location in the forecast.

b. F2 14–16 August assimilation/20–23 August verification

Validating F2 as a 6-day forecast, we found little evidence (Table 2) for quantitative skill when considering the entire model region as the domain of interest. Although a slight reduction in rmse was observed for level 4, the remaining levels all fared poorly compared to persistence in the full domain. In subdomain B, centered on the developed deep-sock meander, the forecast reveals some quantitative skill for both level 4 and level 5 (Table 2), as measured by our defined correlation measure. However, as noted above, the 7-day F2 forecast

TABLE 1. Primitive equation case F2 forecast skill vs persistence.

Assimilating 14–16 August/predicting 18–19 August				
	Zigzag area		Subdomain A	
Temperature at	ACC change	Rmse change	ACC change	Rmse change
25 m	+0.079	+15%	+0.042	+13%
75 m	−0.089	+23%	−0.013	+22%
125 m	−0.042	+11%	+0.005	+10%
sigma 4	−0.030	+5%	+0.025	−2%
sigma 5	−0.083	+30%	−0.050	+16%

TABLE 2. Primitive equation case F2 forecast skill vs persistence.

Assimilating 14–16 August/predicting 20–23 August				
	Full domain		Subdomain B	
Temperature at	ACC change	Rmse change	ACC change	Rmse change
25 m	−0.307	+74%	−0.202	+58%
75 m	−0.119	+41%	−0.218	+73%
125 m	−0.065	+28%	−0.029	+27%
sigma 4	0.000	−3%	+0.101	−20%
sigma 5	−0.018	+8%	+0.033	−10%

successfully forms the cold intrusion feature and, thus, provides a much more useful field estimate for applications than does persistence, although this usefulness is not able to be quantified by our present measure.

c. F5 14–19 August assimilation/20–23 August verification

The quantitative forecast skill for F5 is presented in Table 3, and the results are impressive. When validating over the entire zigzag region, all model levels show increased skill relative to persistence, both in an increased correlation coefficient and in a reduced rmse. Focusing on subdomain B, surrounding the deep sock, Table 3 and Figs. 10 and 11 show that the skill levels drop a bit for the upper two levels but rise even higher for the deeper levels. It is clear that this forecast has substantial quantitative skill.

As discussed previously, the modeled deep-sock meander is in phase with the observed at depth (greater than 50 m) but occurs downstream of the observed near the surface. So we now account for this spatial disparity as a function of model level as shown in Table 4 and Figs. 10 and 11. The solid lines show the forecasting skill for each day of the forecast in subdomain B, validating for the 20–23 August survey. A forecast of persistence of the 18–19 August observations is indicated by the dashed line. The dotted line indicates the maximum skill of the spatially lagged 22 August forecast. For the top level (25 m), the maximum skill occurs when the forecast is shifted 10 km west and 5 km south (one model grid point equaling 5 km). For the 75-m layer, the maximum skill is obtained when shifting the model fields 10 km east and 10 km south, and at 125 m, the forecast must be shifted 10 km south. For the sigma coordinate layers, the shift is 5 km west, 10 km south, for level 4 and only 5 km south for level 5. The fact that all the spatial lags are 10 km or less reveals the high skill of this forecast. Thus, this analysis shows that the model field tends to be somewhat too "equivalent barotropic," in the sense that the observed field at 25 m develops upstream relative to the fields at depth, while the model field tends to develop in phase from top to bottom.

Skillful results were also obtained for upper water column flows using a quasigeostrophic forecast model (Miller et al. 1995b), although the QG model was unable to capture the sharp and narrow features of the hammerhead structure observed in the satellite map (Fig. 5) and PE forecast temperature field (Fig. 9). However, the QG model was validated against dynamic height rather than temperature as accomplished here; a direct comparison between forecast PE and QG current or dynamic height fields has yet to be carried out. But since both the PE and (flat bottom) QG models exhibited upper-ocean forecast skill, we note that topographic influence was minimal during the 3–4 days of the simulations because the modeled instability apparently was trapped in the upper part of the water column. Only the PE model was able to forecast the deep flows around the IFF with fidelity.

7. Discussion and conclusions

From 14–23 August 1993, there occurred in the meandering and eddying IFF system two rapid and en-

TABLE 3. Primitive equation case F5 forecast skill vs persistence.

Assimilating 14–19 August/predicting 20–23 August				
	Zigzag area		Subdomain B	
Temperature at	ACC change	Rmse change	ACC change	Rmse change
25 m	+0.023	−3%	−0.039	−1%
75 m	+0.022	−5%	+0.019	+1%
125 m	+0.044	−11%	+0.060	−12%
sigma 4	+0.072	−21%	+0.100	−27%
sigma 5	+0.078	−30%	+0.160	−43%

TABLE 4. Primitive equation case F5 space-lagged forecast skill vs persistence.

Assimilating 14–19 August/predicting 20–23 August				
	Spatial lag		Subdomain B	
Temperature at	East–west lag (km)	North–south lag (km)	ACC change	Rmse change
25 m	+10	+5	+0.140	−17%
75 m	−10	+10	+0.142	−7%
125 m	0	+10	+0.146	−18%
sigma 4	+5	+10	+0.139	−39%
sigma 5	0	+5	+0.187	−50%

ergetic synoptic dynamical events controlled by intermittent burst baroclinic instability. The frontal jet straightened and shifted and then developed a nonlinear hammerhead meander with Arctic water intruding deeply southward. Real-time operational nowcasting via intermittent optimal interpolation assimilation into a primitive equation model, fused the direct stream of hydrographic data as it became available with a feature model and climatology-based representation of the system. This approach provides a powerful and efficient method to generate what we believe to be a very accurate synoptic description of a region as data are collected. This approach could be further improved by using a more sophisticated assimilation methodology. Forecasts very successfully evolved these features dynamically. Statistical quantities that were introduced to quantify forecast skill (anomaly correlation and rmse) indicate that primitive equation dynamical forecasts significantly exceed persistence for a few days. We believe that these methods will prove generally useful as ocean forecasting progresses and can be further developed to allow for better treatment of phase errors. This is important because small spatial scales and the existence of many structures and features makes quantitative verification of ocean mesoscale variability forecasting challenging.

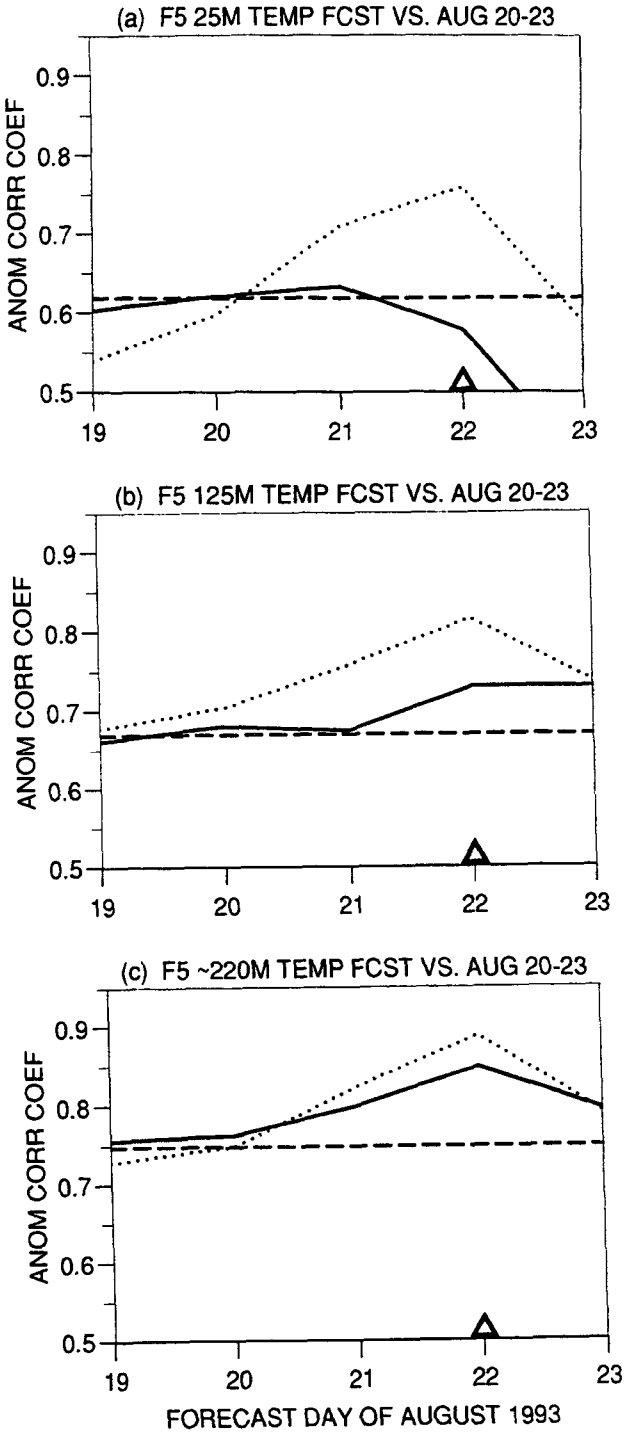

The capability of accurate and efficient real-time nowcasting and forecasting at sea has important implications for ocean science, technology, operations, and management. It makes possible a knowledge of present and future realistic oceanic fields with minimal observational resources. The dataset itself, designed and acquired for a forecast experiment, is of unprecedented quality as a database for regional ocean forecasting research, including observation system simulation experiments to determine minimal resource requirements for field estimates of predetermined accuracy. The data are available as a useful evaluation and verification resource to the ocean forecasting community.

Acknowledgments. The observations discussed in this work were obtained via the skilled data acquisition and processing abilities of the CTD/XCTD/XBT support staff of SACLANTCEN's Applied Oceanography Group, Ocean Engineering Department, and Digital Computer Department, and the captain and crew of the R/V *Alliance*. The Harvard group wishes to thank the following individuals at Harvard University for their efforts in the de-

FIG. 10. Anomaly correlation coefficient between each day of forecast temperature and the observations of 20–23 August for case F5 (14–19 August assimilation) at (a) 25 m, (b) 125 m, and (c) sigma level 4, in the specified area subdomain B (11.2°–8.3°W and 63.7–64.5N). The dashed line corresponds to persistence of observations for 18–20 August. Solid line corresponds to the real-time forecast, which ideally should be a maximum on 22 August (indicated by the triangle). The dotted line corresponds to the spatially lagged forecast that maximizes the correlation on 22 August, as described in text. At 25 m, the maximum correlation occurs when the forecast field is shifted 10 km west and 5 km south, at 125 m, shifted 10 km south, and at sigma 4, shifted 5 km south.

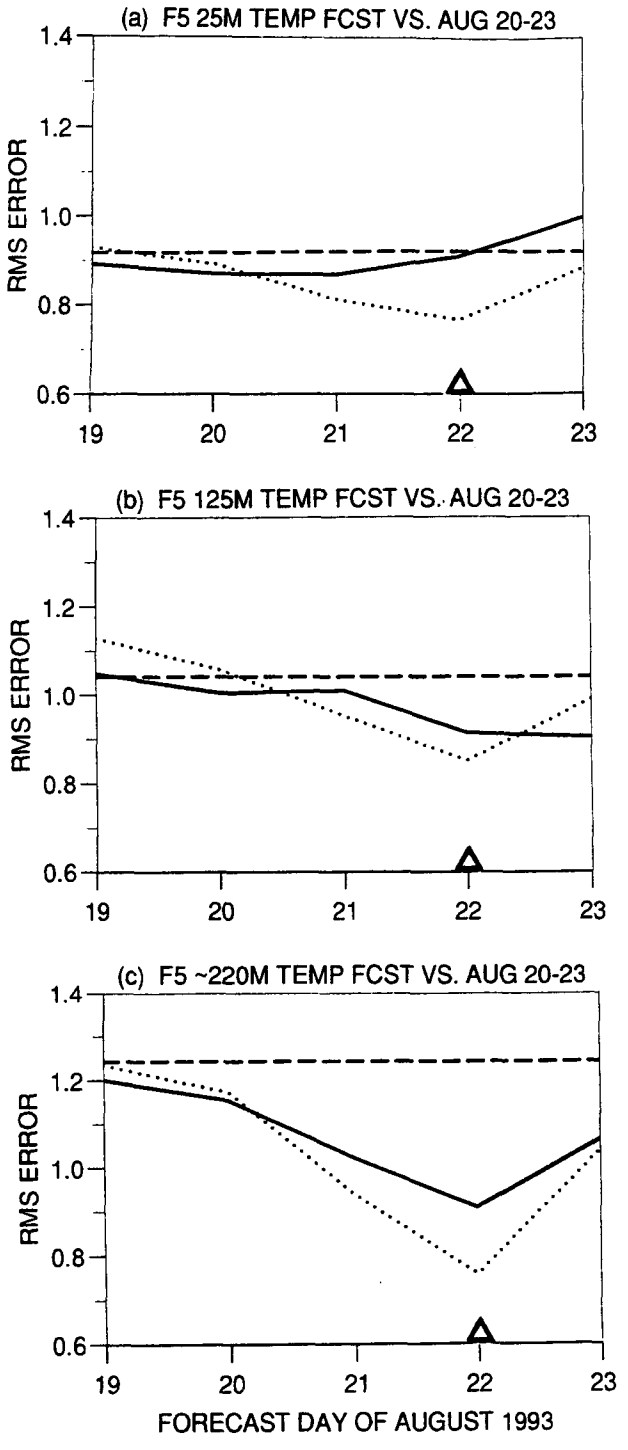

FIG. 11. As in Fig. 10 but for rmse.

velopment and setup of the models used during this experiment: Dr. Patrick J. Haley, Dr. Carlos Lozano, and Mr. N. Quinn Sloan III. Marsha Glass supplied invaluable logistical assistance. AJM was supported by SACLANTCEN during the data acquisition and forecast analysis stages of this work and is supported at SIO by NOAA Grants NA36GPO372 and NA47GPO188. The Fleet Numerical Oceanographic Center (FNOC) provided the NODDS products. This research was supported at Harvard University by the Office of Naval Research under Grants N00014-93-1-0577, N00014-90-J-1612, and N00014-91-J-1521.

References

Allen, J. T., D. A. Smeed, and A. L. Chadwick, 1994: Eddies and mixing at the Iceland–Faroes Front. *Deep-Sea Res.*, **41,** 51–74.

Bennett, T., Jr., J. Boyd, L. Knauer, G. Dawson, and W. Wilson, 1992: A feature model of the Iceland–Faeroe Front. *Mar. Tech. Soc. J.*, **26**(2), 44–52.

Bryan, K., and M. D. Cox, 1967: A numerical investigation of the oceanic general circulation. *Tellus,* **19,** 54–80.

Clancy, R. M., 1992: Operational modeling: Ocean modeling at the Fleet Numerical Oceanography Center. *Oceanography,* **5,** 31–35.

Denbo, D. W., and A. R. Robinson, 1988a: Harvard gapcasts; a progress report: Regional forecasting, processes and methodology in the Iceland–Faeroe Island gap. Part I: Data forecast and hindcast experiments. Reports in Meteorology and Oceanography: Harvard Open Ocean Model Rep., 32, 203 pp. [Available from Division of Applied Sciences, Dept. of Earth and Planetary Sciences, Pierce Hall, Harvard University, Cambridge, MA 02138.]

——, and ——, 1988b: Harvard gapcasts; a progress report: Regional forecasting, processes and methodology in the Iceland–Faeroe Island gap. Part II: GFD and process experiments. Reports in Meteorology and Oceanography: Harvard Open Ocean Model Rep., 33, 218 pp. [Available from Division of Applied Sciences, Dept. of Earth and Planetary Sciences, Pierce Hall, Harvard University, Cambridge, MA 02138.]

Dietrich, G., 1969: Atlas of the hydrography of the northern North Atlantic. Conseil International pour l'Exploration de la Mer. Service Hydrographie, Charlottenlund Slot, Denmark.

Durham, D. L., and J. K. Lewis, 1992: Introduction: Oceanic and atmospheric nowcasting and forecasting. *Mar. Tech. Soc. J.,* **29,** 3–4.

Fuglister, F. C., 1963: Gulf Stream '60. *Progress in Oceanography,* Vol. 1, Pergamon, 265–373.

Glenn, S. M., and A. R. Robinson, 1995: Verification of an Operational Gulf Stream Forecasting Model. *Quantitative Skill Assessment for Coastal Ocean Models, Coastal and Estuarine Studies,* Vol. 47, D. Lynch, Ed., Amer. Geophys. Union, 469–499.

Gould, W. J., J. F. Read, and J. Smithers, 1987: SEASOAR profiles in the Iceland–Scotland area, May 1987. Rep. 253, Inst. of Oceanogr. Sci., Wormley, England, 50 pp.

Hansen, B., and J. Meincke, 1979: Eddies and meanders in the Iceland–Faeroe Ridge area. *Deep-Sea Res.,* **26A,** 1067–1082.

Harvard Group, 1994: HOPS, the Harvard Ocean Prediction System. [Available from Division of Applied Sciences, Dept. of Earth and Planetary Sciences, Pierce Hall, Harvard University, Cambridge, MA 02138.]

Hopkins, T. S., 1991: The GIN Sea—A synthesis of its physical oceanography and literature 1972–1985. *Earth-Sci. Rev.,* **30,** 175–318.

Lai, C.-C. A., W. Qian, and S. M. Glenn, 1994: Data assimilation and model evaluation datasets. *Bull. Amer. Meteor. Soc.,* **75,** 793–809.

Lozano, C. J., P. J. Haley, H. G. Arango, N. Q. Sloan, and A. R. Robinson, 1994: Harvard coastal/deep water primitive equation model. Reports in Meteorology and Oceanography: Harvard Open Ocean Model Reports, 15 pp. [Available from Division of Applied Sciences, Dept. of Earth and Planetary Sciences, Pierce Hall, Harvard University, Cambridge, MA 02138.]

Miller, A. J., H. G. Arango, A. R. Robinson, W. G. Leslie, P.-M. Poulain, and A. Warn-Varnas, 1995a: Quasigeostrophic forecasting and physical processes of Iceland–Faeroe Front variability. *J. Phys. Oceanogr.*, **25,** 1273–1295.

——, P.-M. Poulain, A. R. Robinson, H. G. Arango, W. G. Leslie, and A. Warn-Varnas, 1995b: Quantitative skill of quasi-geostrophic forecasts of a baroclinically unstable Iceland–Faeroe Front. *J. Geophys. Res.*, **100,** in press.

——, P. F. J. G. Lermusiaux, and P.-M. Poulain, 1995c: A 1.8-day topographic Rossby mode resonance trapped to the Iceland–Faeroe Ridge. Preprints, *10th Conf. on Atmospheric and Oceanic Waves and Stability,* Big Sky, MT, Amer. Meteor. Soc., 19–20.

Mooers, C. N. K., A. R. Robinson, and J. D. Thompson, 1986: Ocean prediction workshop 1986. A status and prospectus report on the scientific basis and the navy's needs. *Proc. Ocean Prediction Workshop,* Parts I and II, Cambridge, MA and Long Beach, MI, Institute for Naval Oceanography, NSTL, MS, 486 pp.

Niiler, P. P., S. Piacsek, L. Neuberg, and A. Warn-Varnas, 1992: Sea surface temperature variability of the Iceland–Faeroe Front. *J. Geophys. Res.*, **97,** 17 777–17 785.

Peggion, G., 1991: Diagnostic calculations for the reconstruction of environmental and acoustic conditions in the Iceland–Faeroe Ridge region during June 1989. SACLANTCEN SR-178, 65 pp. [Available from SACLANT Undersea Research Centre, 19138 La Spezia, Italy.]

Peloquin, R. A., 1992: The navy ocean modeling and prediction program. *Oceanography,* **5,** 4–8.

Perkins, H., 1992: Large-scale structure of the Iceland–Faeroe Front. SACLANTCEN SR-189, 40 pp. [Available from SACLANT Undersea Research Centre, 19138 La Spezia, Italy.]

Poulain, P.-M., 1992: Cruise report for R/V *Alliance* cruise: GIN92, Greenock-Liverpool, 13–29 October 1992. 29 pp. [Available from SACLANT Undersea Research Centre, 19138 La Spezia, Italy.]

——, 1993: Cruise report for R/V *Alliance* Cruise: GIN93, Wilhelmshaven-Bodo, 11–26 August 1993. 33 pp. [Available from SACLANT Undersea Research Centre, 19138 La Spezia, Italy.]

Read, J. F., and R. T. Pollard, 1992: Water masses in the region of the Iceland–Faeroe Front. *J. Phys. Oceanogr.*, **22,** 1365–1378.

Robinson, A. R., Ed., 1983: *Eddies in Marine Science,* Springer-Verlag, 609 pp.

——, 1992: Shipboard prediction with a regional forecast model. *Oceanography,* **5,** 42–48.

——, 1993: Physical processes, field estimation and interdisciplinary ocean modeling. Reports in Meteorology and Oceanography: Harvard Open Ocean Model Rep. 51. 80 pp. [Available from Division of Applied Sciences, Dept. of Earth and Planetary Sciences, Pierce Hall, Harvard University, Cambridge, MA 02138.]

——, S. M. Glenn, M. A. Spall, L. J. Walstad, G. M. Gardner, and W. G. Leslie, 1989: Forecasting Gulf Stream meanders and rings. *Trans. Amer. Geophys. Union,* **70**(45), 1464–1473.

——, and Coauthors, 1994: Real-time nowcasting and forecasting R/V *Alliance* GIN 93 Cruise 11–26 August 1993 operational forecasts and simulation experiments at sea. Reports in Meteorology and Oceanography: Harvard Open Ocean Model Rep. 50, XXX pp. [Available from Division of Applied Sciences, Dept. of Earth and Planetary Sciences, Pierce Hall, Harvard University, Cambridge, MA 02138.]

Scott, J. C., and N. A. Lane, 1990: Frontal boundaries and eddies on the Iceland–Faeroe Ridge. *Proceedings on Ocean Variability and Acoustic Propagation,* J. Potter and A. Warn-Varnas, Eds., Kluwer Academic, 449–461.

——, and A. L. McDowall, 1990: Cross-frontal cold jets near Iceland: In-water, satellite infrared and GEOSAT altimeter data. *J. Geophys. Res.*, **95,** 18 005–18 014.

Semtner, A. J., 1974: An oceanic general circulation model with bottom topography. Tech. Rep. 9, Department of Meteorology, University of California, Los Angeles, 99 pp.

Smart, J. H., 1984: Spatial variability of major frontal systems in the North Atlantic Norwegian Sea area: 1980–1981. *J. Phys. Oceanogr.*, **14,** 185–192.

Spall, M. A., and A. R. Robinson, 1989: A new open ocean, hybrid coordinate primitive equation model. *Mathematics and Computers in Simulation,* **31,** 241–269.

Willebrand, J., and J. Meincke, 1980: Statistical analysis of fluctuations in the Iceland–Scotland frontal zone. *Deep-Sea Res.,* **27A,** 1049–1066.

Willems, R. C., and Coauthors, 1994: Experiment evaluates ocean models and data assimilation in the Gulf Stream. *Trans. Amer. Geophys. Union,* **75,** 34.